Complex voltammetric and fractal study of adsorbed layer's structure of pure Triton-X-100 and in mixture with *o*- or *p*-nitrophenol

Blaženka Gašparović*,[1], Dubravko Risović[2], Božena Ćosović[1]

[1]*Center for Marine and Environmental Research,* [2]*Molecular Physics Laboratory,*

Ruđer Bošković Institute, POB 180, HR-10002 Zagreb, Croatia

Abstract

Adsorption of well-known surfactant Triton-X-100 (T-X-100) and mixed systems comprising T-X-100 with *o*- or *p*-nitrophenols, at the mercury/electrolyte solution interface *vs*. T-X-100 bulk concentration has been studied. Diversified approach comprising capacitive current measurements, desorption peak height analysis, fractal analysis, nonthermodynamic calculation of coefficient of lateral interaction, calculation of relative coverage assuming flat and perpendicular dispositions of molecules, fit with Flory-Huggins isotherms corresponding to different molecular orientations, and predictions of Random Sequential Adsorption (RSA) and equilibrium (generalized RSA) theories, together with analysis of reduction mechanisms of nitrophenols has been used.

It is found that the adsorbed layer of T-X-100 and mixed layers are fractal. Fine structural changes of adsorbed layer(s) are identified and related to corresponding changes in fractal dimension. Evidence derived from *ac* and *sw* voltammetric measurements and theoretical considerations support these conclusions. For the adsorption of T-X-100 four different adsorption phases, corresponding to increasing bulk concentration, are identified and characterized. Mixed systems undergo different changes in microstructure that are

reflected in observed changes of reduction mechanisms of nitrophenols. Those are in turn related to the differences in molecular interactions between T-X-100 and certain nitrophenol. The results are relevant for study of any system exhibiting fractal features and accessible to electrochemical methods such as adsorbed films, models of biological membranes, etc.

Keywords: adsorption and reduction, fractal analysis, voltammetry, Triton-X-100, *o*- and *p*-nitrophenol

∗ Corresponding author. Tel: +385-1-4561-148; fax: +385-1-4680-242

E-mail address: gaspar@rudjer.irb.hr

1. Introduction

The adsorption processes and structure properties of adsorbed films are subjects of interest in different fundamental and applied scientific and technological areas studied by different theoretical methods and experimental techniques. The electrochemical approach is wide spread due to possibility of investigation of different phase boundaries and interface processes. On the other hand, since adsorbed layers may have fractal structure [1, 2] their characteristics can be described and understood in terms of fractal geometry [3]. Fractal analysis was found to be powerful tool to follow adsorbed layer build up on a molecular level, whenever molecular reorientation and/or formation of patches and/or layer restructuring takes place [1, 4].

The fractal analysis approach is based on the possibility to describe quantitatively complex objects that are statistically scale-invariant. This property is manifested in a power-law-scaling ratio that characterizes one or more of the features of an object or a process carried out near or at the object:

$$\text{Feature} \sim \text{scale}^{\Delta} \tag{1}$$

Here "feature" and "scale" are considered in the broadest sense, and the non-integer exponent Δ ("effective fractal dimension") is a parameter, that indicates how sensitive the considered feature is to changes in the applied scale. Recently, based on this principle the method of hanging mercury drop electrode scaling was developed for determination of fractal dimension, D, of adsorbed layer [1]. In this method the used "feature" is capacitive current and "scale" is the electrode surface area expressed through the radius of hanging mercury drop. Hence,

$$i_c \propto r^D \tag{2}$$

or expressed through spherical electrode surface area:

$$i_c \propto A^{D/2} \tag{2a}$$

This relation has its roots in the fact that permittivity and derived quantities of any fractal structure scale as ~ R^{D-d}, where R is the structure size (extent) and d the Euclidean dimension of embedding space [5]. Consequently, the specific capacitance C_s, scales as $C_s \sim r^{D-2}$. Since the differential capacitance of the interface is given by $C_D = AC_s$, and as $i_c \sim C_D$, with $A \sim r^2$, we again get Eq. (2).

However, although Eq. (1) is generally valid, and often used, one must be cautious in its use and interpretation of power-law dependence as sign of fractality [6,7]. Because, mathematically speaking, power-law scaling is necessary but not sufficient condition: power-low dependence of some feature on scale does not necessarily mean that the underlying structure is self-similar and that D has geometrical meaning. It is therefore necessary to verify assumptions of geometric self-similar structure and evaluate the cutoffs of scaling regime [8]. In spatial fractals, the scaling range is limited by the size of the basic building blocks and the system size and it is usually further reduced due to system or apparatus limitations or properties.

The study of organic substance adsorption is important also due to the fact that organic substances in aquatic media modify all phase boundaries. The organic adsorbed layers may have selective permeability for other molecules and ions and such modified boundaries could facilitate coadsorption of other organics. In such systems both electrostatic and/or hydrophobic interactions can take place influencing the layer characteristics. The structure of the adsorbed layer and adsorption kinetics depend on the

interactions between molecules themselves and with the surface, and on external forces applied during the adsorption. Also, the kinetics of reduction on the electrode surface is influenced by the presence of adsorbed organic molecules and can be correlated with the microstructure of the adsorbed layer. Hence, it is of interest to get insight into the morphology, structural changes, build-up mechanisms, and involved interactions in and at the layer.

In this paper, voltammetric and fractal analysis have been used to study complex adsorption of system comprising nonionic surfactant Triton-X-100 (T-X-100) and *o*- or *p*-nitrophenol (ONP and PNP, respectively). T-X-100, $(CH_3)_3C\text{-}CH_2\text{-}C(CH_3)_2\text{-}C_6H_4\text{-}(OCH_2CH_2)_{9\text{-}10}\text{-}OH$, a well-known commercial surfactant, was selected due to its wide use in different areas, as in polarography [9-12], petroleum industry [13], etc. Nitrophenols are known to be pollutants that appear in the natural aquatic systems [14], and are included on the list of priority pollutants of the Environmental Protection Agency [15]. The chosen nitrophenols were selected to investigate influence of molecular geometry (substituent position) on mixed layer structure and build-up. The observed changes of the electrochemical reduction of nitrophenols in the presence of adsorbed T-X-100 are connected to microstructure of adsorbed layer and to the transformations during its build-up. Competitive adsorption at different bulk concentration has been studied and explained in terms of structural changes of mixed adsorbed layers.

2. Experimental

The nonionic surfactant T-X-100 is highly hydrophobic (calculated octanol/water partition constant, log K_{OW} = 4.1 [16]) and has a great tendency to adsorb onto surfaces influencing mass and energy transfer across the modified interface. The adsorption of T-X-100 has been found to be diffusion-controlled [17]. Its critical micellar concentration (CMC) in 0.5 M NaCl is 1.41 x 10^{-4} M i.e. ~ 85 mg/dm^3 [18]. ONP and PNP are few orders of magnitude less hydrophobic than T-X-100, the octanol/water partition coefficients for ONP and PNP are: log K_{OW} = 1.89 and 2.04 for neutral species, respectively, and the corresponding values for the ionic species are – 1.77 and – 1.76 [19]. The ONP and PNP pK_a values are 7.23 and 7.08, respectively [19]. Their adsorption on the electrode is in general characterized by the presence of the aromatic moiety. The energetic adsorbate-mercury electrode interaction is usually expressed through the standard adsorption Gibbs energy $\Delta G°_{ads}$. The experimental $\Delta G°_{ads}$ values are always related to a planar disposition of the aromatic molecule on the metal surface, and the mean $\Delta G°_{ads}$ for 38 aromatic compounds was found to be –25 kJ/mol [20] indicating physisorption. This free energy of adsorption is higher than that of T-X-100 (≈ - 36 kJ/mol, as calculated from the adsorption coefficient from ref [17]).

For the study of adsorption of T-X-100, phase sensitive alternating current (*ac*) voltammetry (90° out of phase) was used. For the study of the oxidation-reduction processes of the ONP and PNP, without and in the presence of T-X-100, phase sensitive *ac* (in phase mode) and square wave (sw) voltammetry were used.

Ac and *sw* voltammetric measurements were performed by AUTOLAB with PGSTAT 20 (Ecochemie, Netherlands). The frequency of the *ac* voltage was 170 Hz, the amplitude 0.010 VMS, potential step 0.0021 V, interval time 0.29 s and modulation time was 0.19 s. For *sw* voltammetry frequency was 170 Hz, step potential 2.1 mV and amplitude was 0.02 V. All experiments were performed in a three-electrode system. Working electrode was hanging mercury drop (Metrohm, Switzerland), with Ag/AgCl/3 M KCl electrode as the reference and a platinum wire as the auxiliary electrode. All measurements were performed under stirring of the solution (270 r.p.m.), at the potential of –0.35 V, with 1 min accumulation prior to the potential scan.

The fractal dimension, *D,* is determined from the slope of the log-log plot of i_c *vs*. *A* obtained from the size scaling of the hanging mercury drop electrode [1]. Measurement was performed each time with a freshly prepared new drop of a selected size that was not changed during the measurement.

For the purpose of the adsorption analyses the measurements were performed in the potential range E = - 0.35V to – 1.85 V. The values of differential capacitance were calculated from the measured capacity current. The calibration was done using a series of known capacitors (polypropylene-type, precision ± 1%, mfg. "Iskra"). The adsorption of T-X-100 was studied in a concentration range of 0 - 10 mg/dm^3 (0 - ~1.7 10^{-5} M). The adsorption in mixed systems (T-X-100 + ONP or PNP) and study of oxido-reduction processes of the nitrophenols in presence of T-X-100 were studied for 10^{-4} M solution of nitrophenols and changing T-X-100 concentration in the range 0 - 10 mg/dm^3. In the study of oxido-reduction processes the applied potential was in the range of E = - 0.35V to – 1.0

V. Pure nitrogen was used for deaeration of the solutions in the faradic current measurements.

T-X-100 (Rohm and Haas, Italy) and ONP and PNP (Sigma, USA) were used without further purification. Mercury was purified by double distillation under reduced pressure. $NaHCO_3$ (Merck) was used without prior purification. NaCl (Kemika, Croatia) was purified by prolonged heating at 450°C. All solutions were prepared with deionised water obtained with the Milly-Q Water System (Millipore, Switzerland). Carbonate buffer was used to maintain pH 8.3.

3. Results and discussion

In Fig. 1 log-log plot of measured capacitance current vs. electrode area for pure electrolyte and representative T-X-100 concentration are depicted. According to the Eq. 2a the slope of the line gives the fractal dimension. The fractal dimension is elaborated for electrode potential – 0.35 V at which there is no oxido-reduction processes of nitrophenols. For the purpose of fractal analysis in the voltammetric measurements the electrode surface area of the mercury drop was varied stepwise over nine sizes in the range of 0.9 to 3.8 mm^2.

Adsorption of Triton-X-100

Adsorption of T-X-100 has been studied by *ac* voltammetry, out of phase mode. Resulting differential capacitance *vs.* applied potential curves for increasing bulk T-X-100 concentrations are shown in Fig. 2. For comparison the capacitance curves of ONP and PNP, (labeled in Fig. 2 as *ONP* and *PNP*, respectively) are added. At E = - 0.35 V and at the bulk concentration of 10^{-4} M, higher decrease of the differential capacitance is observed for PNP in comparison to that of ONP. Since there is no change in differential capacitance of ONP and PNP, for different adsorption times, we have assumed that adsorption of nitrophenols is practically instantaneous.

The shapes of T-X-100 capacitance curves (cf. Fig. 2) indicate that, at least at the investigated concentrations, T-X-100 does no form compact layer that is characterized by appearance of capacitance pit [21]. Also, chronoamperometric measurements had not provided any evidence of nucleation processes [22]. Such behavior is usually associated with the transformation of an adsorbed layer that consists of close-packed patches of associated adsorbate molecules, rather than continuos single entity layer [23, 24].

T-X-100 is strongly adsorbed over wide range of potentials both at positively and negatively charged mercury electrode surface. In the bulk T-X-100 concentration range up to 5 mg/dm^3 one desorption peak was recorded at $E \approx$ - 1.6 V, associated with monomer desorption [25]. The second desorption peak recorded at $E \approx$ -1.8 V for concentrations above 5 mg/dm^3 is attributed to the adsorption-desorption of dimers [25]. The height of the first desorption peak is proportional to the logarithm of T-X-100 bulk concentration, that is usually associated with simple adsorption/desorption processes of monomers. In Fig. 3 we can identify four concentration ranges with different proportionality constants indicating different adsorption stages. First three ranges comprising bulk T-X-100 concentrations up

to 4 mg/dm^3 are characterized with positive proportionality constant, while for higher concentrations the trend reverses as the height of this first peak decreases due to the adsorption/desorption of the T-X-100 dimers. The observed capacitance minimum is 3.11 μF/cm^2.

In order to determine the fractal dimension of the adsorbed T-X-100 layer the capacitive current data obtained by phase sensitive *ac* voltammetry were subjected to a fractal analysis. For pure electrolyte it was obtained that $D = 2.02 \pm 0.02$ indicating smooth nonfractal electrode surface.

The changes of the fractal dimension during adsorbed T-X-100 layer build-up are compared to the corresponding apparent adsorption isotherm. Results are presented in the Figs. 4a and b, curves 1. The apparent adsorption isotherm, depicted in Fig. 4b was obtained from the measured capacitive current i_c *vs*. T-X-100 bulk concentration. The corresponding fractional electrode coverage, θ, was determined from the measured capacitive current, i_c, vs. T-X-100 concentration from the following relation:

$$\theta = \frac{i_0 - i_c(\theta)}{i_0 - i_c(\theta = 1)} \tag{3}$$

Here, i_0 represents the capacitive current corresponding to the interface capacitance without organic molecules, $i_c(\theta)$ the capacitive current in the presence of adsorbed organic molecules and $i_c(\theta=1)$ the capacitive current obtained for the totally covered electrode.

To describe the adsorption process of T-X-100 we have used the Frumkin isotherm [26] that includes adsorbate-adsorbate interaction, and is given by:

$$\frac{\theta}{1-\theta} e^{-2a\theta} = Bc \tag{4}$$

Here, a is the interaction coefficient, c is the bulk concentration of the adsorbate and B is the adsorption constant.

However, data points in Fig. 4b representing θ calculated from Eq. (3) are connected with B-spline fit and not with Frumkin – type isotherm (sigmoidal fit). This has been done in order not to smooth out, but rather to emphasize finer features related to the adsorption process, such as slight "knee" in apparent isotherm. Based on fractal analysis the similar "knee" observed in the case of linoleic acid adsorption was attributed to the onset of reorientation [1]. The observed slight decrease in coverage with increase of concentration, around $C_{T\text{-}X\text{-}100} \approx 0.25$ mg/dm^3 ("knee") could be explained as a consequence of onset of erection of initially flatly adsorbed molecules that by erecting provide more free space for adsorption, resulting in apparent decrease of the relative electrode coverage.

The Fig. 4a, curve 1, shows that adsorbed layer of T-X-100 exhibit fractal properties, hence, arranges itself in a self-similar way even at low fractional electrode coverage. The experimental data presented in this figure are purposefully left "raw" i.e. no smoothing has been applied, and data are fitted with B-spline, consequently resulting in some minor peaks that are probably just experimental scatter. This has been done in order to preserve some not so prominent features that might come out as significant in subsequent analysis. In a first stage of adsorption process D increases gradually with increase of bulk concentration up to 0.2 mg/dm^3 ($\theta \sim 0.35$) while molecules probably adsorb flatly in a similar way but progressively more dense, due to the reduction of space available for adsorption. In the T-X-100 concentration range between 0.2 and 0.8 mg/dm^3 the fractal dimension changes considerably, exhibiting two prepeaks and pronounced main peak. Here, reduction of available space on the electrode surface, combined with molecular

lateral interactions, forces adsorbed molecules to erect. This reorientation is reflected in rapid increase of fractal dimension up to value $D = 2.62$, observed at T-X-100 bulk concentration of 0.4 mg/dm^3 (~ 6.7 x 10^{-7} M), corresponding to ~ 80 % fractional electrode coverage. However, the process of erection is not instantaneous and not limited to the specific concentration, but rather spread over finite concentration range, characterized with relatively broad main fractal peak. The hypothesis of molecular erection can be also checked considering the thickness of adsorbed layer. Rod-like molecules, such as T-X-100; form a thinner layer when flatly adsorbed than when adsorbed in slant or erected position. Indeed, evaluation of average layer thickness of adsorbed T-X-100 at bulk concentration of 0.26 mg/ dm^3 yields thickness of about 1.7 nm [5], a value that is much higher than the estimated T-X-100 "diameter" (about 0.7 nm). This average layer thickness value indicates that at this concentration all molecules are not adsorbed flatly (in compliance with theoretical predictions, cf. Fig 5b) and are partly adsorbed perpendicularly or in slant position. This complies with finding of Guidelli and Moncelli [27] that, for concentrations bellow 10^{-4} M, T-X-100 is adsorbed in a monolayer with an orientation intermediate between the flat and the perpendicular with alkyl end of the molecule in contact with electrode. The end of adsorbed layer transformation is indicated by the decrease of fractal dimension to a value slightly above 2. In the next concentration range, up to 4 mg/dm^3 (6.7 x 10^{-6} M), D remains practically constant with average value ≈ 2.05 indicating that adsorption proceeds with molecules adsorbed perpendicularly in a relatively homogenous layer. Second increase of fractal dimension, obtained at T-X-100 bulk concentrations higher than 4 mg/dm^3, coincides with adsorption of T-X-100 dimers [25]. Adsorption of dimers causes loss of homogeneity and increase of fractal dimension to $D \leq 2.14$.

The four concentration ranges of T-X-100 identified with fractal analysis and characterized by different behavior of D coincide with concentration ranges identified in the analysis of the first desorption peak height (Fig. 3). These ranges are related to the four different adsorption stages. First three are related to the adsorption of monomers as follows: initially flatly adsorbed molecules, transformation stage, and adsorption in the perpendicular position. The fourth stage, appearing at the highest investigated bulk concentrations, corresponds to adsorption of dimers. This analysis shows complexity of the adsorption process of T-X-100, also observed in an earlier study by Batina *et al* [17]. The observed deviation from their model of adsorption process was attributed to rate-determining step in the overall mechanism caused by reorientation of adsorbed molecules or formation of several adsorbed layers. Fractal analysis approach facilitates resolution of such problems by providing evidence that the reorientation of adsorbed molecules indeed takes place in certain fractional electrode coverage range.

The observed changes of fractal dimension with increase in T-X-100 bulk concentration are a consequence of structural changes in the adsorbed layer. These structural changes are in turn related to changes of molecular interactions between adsorbed molecules. Theoretically these interactions are included in a Frumkin type isotherm (Eq. (4)) through the coefficient of lateral interaction, a. This coefficient was calculated from measured data applying method described elsewhere [1, 26]. Due to the non-equilibrium conditions in the experiment, the results, although obtained using a nonthermodynamic method, should be interpreted cautiously. However, we think that they do reflect, at least qualitatively, the nature of lateral interaction between the molecules during the adsorption process. Although, $\lim_{\theta \to 0.5} a = 2$, one must be cautious in evaluating the value of a at θ

exactly 0.5 due to possible numerical errors. However, this is not relevant for our considerations that are qualitative. Fig. 5a shows the variations of the coefficient of lateral interaction, *a*, with increasing T-X-100 bulk concentration. The change in coefficient *a* corresponds to before discussed adsorption stages. In the first stage coefficient *a* is positive and changes very slowly. In the second adsorption stage an abrupt change of *a* appears around bulk concentration of 0.3 mg/dm^3. This "discontinuity" of *a,* that lies in the concentration range where the onset of major changes in D takes place, is attributed to the structural transformation(s) of the layer. The next stage in which adsorption proceeds with molecules adsorbed in the erected position forming relatively homogenous layer ($D \approx 2$), is characterized by a positive and increasing coefficient of lateral interaction. The similar range of values for the attractive coefficient of lateral interaction was obtained, albeit by different methods, for the adsorption of T-X-100 on dropping mercury electrode [27].

The observed changes can be better understood considering disposition of adsorbed molecules on the electrode surface. Calculation of fractional electrode coverage with horizontally and perpendicularly adsorbed molecules in dependence on the T-X-100 bulk concentration can be accomplished on the basis of the experimentally determined surface coverage as described elsewhere [1, 26]. The results are presented in Fig. 5b. In a concentration range corresponding to low fractional electrode coverage T-X-100 molecules are adsorbed almost exclusively in a flat position probably forming patches due to attractive lateral interactions. The contribution of flatly adsorbed molecules to the fractional electrode coverage continues to increase up to the transition point at which the contribution of perpendicularly adsorbed molecules supersedes that of flatly adsorbed. From that point on, the adsorption proceeds with dominant erected orientation. The onset of the reorientation

can be estimated from the point (concentration or coverage) at which the number of horizontally adsorbed molecules reaches maximum and starts to decrease (due to erection process), this corresponds to $C \approx 0.26$, i.e. $\theta \approx 0.51$ (cf. Fig. 5b). In fractal domain this corresponds to maximum value of prepeak ($D \approx 2.3$). The reorientational process (erection) is not instantaneous, but extends through certain finite coverage range, and is accompanied by corresponding changes in fractal dimension, that after slight decrease increases up to the main fractal peak ($D \approx 2.6$). The end of erection is marked with decrease from maximum value of main fractal peak to the near constant value of fractal dimension corresponding to more uniform and compact layer. In this concentration range the contribution of flatly adsorbed molecules is negligible.

The reorientation (erection) should be also manifested in the adsorption isotherm. The flatly or perpendicularly adsorbed molecules due to the different cross-sectional area in contact with the electrode surface displace different number of solvent molecules. This effect is efficiently accounted for by using modified Flory-Huggins (F-H) isotherm [28, 29], that, besides the coefficient of lateral interaction includes an additional parameter n that describes the number of solvent molecules displaced by one adsorbing molecule. Hence, instead of Eq. (4) we have:

$$\frac{\theta}{n(1-\theta)^n} e^{-2a\theta} = Bc ,$$

an isotherm convenient for interpretation of adsorption of a substance in two different orientations. However, in assigning a value to the parameter n one must be aware that the water molecules are displaced from the surface in clusters corresponding to area of 0.3-0.4 nm^2 [30]. Flat lying T-X-100 molecule occupies an area of approximately 1.63 nm^2 [31].

Based on this we may expect the value of parameter n in F-H isotherm to be $n \approx 4$. The projected area of vertical linear hydrocarbon chain amounts to ~ 0.21 nm^2 [32], hence we may expect that for perpendicularly oriented T-X-100 molecules the values of parameter n in F-H isotherm would be at least $n \approx 0.5$. Fig. 6 shows fit of experimental adsorption isotherm with two F-H isotherms corresponding to low and high concentration ranges. The intermediate coverage range that is transitional in regard to the reorientational transformation and was not included in the fitting procedure. The adsorption in the low concentration (coverage) range ($C \leq 0.15$ mg/dm^3) (where flat orientation predominates) is well approximated ($R^2 = 0.926$) with F-H isotherm with $n = 2.3$, $a = 1.08$ and $B = 5.8 \times 10^5$ mol^{-1}. In the high concentration (coverage) range ($C > 0.4$ mg/dm^3) the corresponding best-fit F-H parameters are $n = 0.44$, $a = 1.92$, $B = 2.24 \times 10^5$ mol^{-1} ($R^2 = 0.888$). The coefficients of lateral interaction obtained from F-H isotherm fitted to experimental data are in perfect agreement with average values of a for the respective concentration ranges obtained from experimental isotherm independently by nonthermodynamic calculation (cf. Fig. 5a). The value of parameter n obtained for the high coverage range is in good agreement with the value predicted for perpendicular adsorption. Lower value of n obtained for low concentration range ($C < 0.2$ mg/dm^3) in respect to that predicted for flat adsorption, may be attributed to the fact that even in this low concentration range a not negligible fraction of molecules is adsorbed in perpendicular or slant position (cf. Fig 5b) resulting in lower average n-value. Hence, we may conclude that at low relative electrode coverage the molecules are adsorbed predominantly in flat position, while at high relative electrode coverage the molecules are adsorbed in perpendicular position.

To get some additional insight into the structural changes during the adsorption process through comparison with theoretical predictions we shall approximate the T-X-100 molecule with a rigid rod with aspect ratio k = 5.6 ($k = l/w$, where l and w are length and width of the "rod"). This approximation is justified by the shape of molecule comprising hydrophobic "head"-group and hydrophilic chain with 9 or 10 ethylene oxide segments, with average total length of molecule, $l \approx 3.9$ nm and width, $w \approx 0.7$ nm. Under the assumption of a random sequential adsorption (RSA) of rigid rods [33] in the two-dimensional space the jamming limit or saturation coverage, θ_S, depends on aspect ratio k, of model rods. The larger the aspect ratio k the lower the jamming limit. RSA Monte Carlo simulations for k = 4 and 6 give saturation coverage θ_S =0.74 and θ_S =0.59, respectively [34]. For a rod like molecule of aspect ratio close to that of T-X-100 the jamming limit estimated from interpolation of cited Monte Carlo simulation results is θ_S = 0.5 (RSA). Contrary to the assumption of RSA model, the generalized RSA or equilibrium model [35] permits limited movement of molecules upon adsorption and consequently another phenomena, namely planar isotropic to nematic transition. The isotropic to nematic (*I-N*) transition coverage $\theta_{I\text{-}N}$ is also aspect ratio dependent. Application to molecules with k = 5.6 gives $\theta_{I\text{-}N}$ = 0.62.

In order to check the applicability of these theoretical considerations for adsorption of T-X-100 in Fig. 7 the dependence of fractal dimension and coefficient of lateral interaction on θ (curves D and a, respectively) are presented. It can be seen that the pronounced changes of fractal dimension and coefficient a appear in the coverage range corresponding to theoretically predicted θ_S and $\theta_{I\text{-}N}$. Hence, the observed changes of D and a could be associated with transitional processes [36], namely, reaching the jamming limit

and isotropic to nematic orientational transition. Additional pronounced change of D is associated with reorientation of molecules from flat to perpendicular position.

In the RSA model in isotropic phase of adsorption the coefficient of lateral interaction should be positive, and gradually increase up to the saturation limit. On the other hand, the fractal dimension should also increase with increased coverage (density). Hence, one should expect that the saturation limit shall be marked with maximum in *a* and *D*. Inspection of Fig. 7 shows that indeed the theoretical jamming limit lies in vicinity of maxima of *D*-prepeak and *a*. The saturation coverage determined from the *a* and *D* is at $\theta_{S(T\text{-}X\text{-}100)} \approx 0.5$ This value complies with the predicted RSA value $\theta_S = 0.5$.

On the other hand, the predicted isotropic-to-nematic transition point lies in vicinity of coverage at which the rate of change of coefficient of lateral interaction after return to positive values has decreased and stabilized (inflection point of *a*-curve in Fig. 7), indicating structurally ordered layer. At this point the fractal dimension exhibits local extreme. Hence, the isotropic to nematic transition seems to occur at $\theta_{I\text{-}N.} \approx 0.6$.

Based on these findings the transformation of the layer should go like this: initially, the attractive forces between molecules that are mostly lying, are responsible for formation of isotropic patches. As the coefficient of lateral interaction slowly increases the density of adsorbed molecules increases up to the jamming limit, characterized by high positive *a*-value and the fractal prepeak. After the jamming limit has been reached, sudden reverse of *a* to negative values, corresponding to strong repulsive interaction, indicates onset of major structural changes: transition from isotropic to nematic structure representing planar reorientation and simultaneously accompanied by process of 3d reorientation from flat to erected adsorption. Isotropic to nematic transition is completed at $\theta_{I\text{-}N.} \approx 0.6$. On the other

hand, the erection of molecules continues after the transition point as indicated by the further change in *D*, and is finished when fractal dimension decreases from maximum to the nearly constant value. After the reorientation has been completed further adsorption continues in erected orientation resulting in relatively homogeneous layer of $D \approx 2$.

Adsorption of mixed systems: T-X-100+ ONP and T-X-100 + PNP

Oppositely to the T-X-100, the adsorbed layers of pure nitrophenols do not exhibit fractal properties at investigated concentration and at potential – 0.35 V. The values of fractal dimension obtained for pure ONP and PNP adsorbed layers are 1.98 and 1.99 (± 0.02), respectively.

The fractal dimensions of mixed systems for T-X-100 with addition of 10^{-4} M ONP or PNP are shown in Fig. 4a, curves 2 and 3, respectively. The corresponding isotherms are given in Fig. 4b, curves 2 and 3, respectively. The differences in *D* of the mixed systems in comparison to the pure T-X-100 are most pronounced in the concentration range that corresponds to low and moderate fractional electrode coverage at which the main fractal peak appears and transformation of T-X-100 adsorbed layer takes place. The T-X-100 layer formed in the presence of ONP is subject to similar transformation as that of pure T-X-100, although somewhat subdued. In the case of mixed layer with PNP the fractal picture is quite different. The observed peaks are substantially reduced in comparison to that of pure T-X-100. The fractal structures generated in presence of repulsive interactions are generally characterized with lower fractal dimension in comparison to the system with attractive

interactions. Hence, the substantial decrease of fractal dimension observed for mixed system, in comparison to that of pure T-X-100, can be attributed to the repulsive interactions between PNP and T-X-100. The reduction of *D* is most pronounced for the main peak associated with molecular reorientation of T-X-100. Hence, we may conclude that in the mixed adsorbed layer of T-X-100 with PNP the reorientation of T-X-100 from flat to-perpendicular position is not the dominant process. This could indicate that T-X-100 molecules are adsorbed mostly in the perpendicular position even at low fractional electrode coverage as probably indicated with a fractal peak appearing at C≈ 0.15 mg/dm^3. At low bulk concentrations of T-X-100, the respective electrode coverage in a mixed system is high ($\theta \approx 0.3$) due to major contribution to the electrode coverage from PNP molecules that are supposed to adsorb flatly [20]. Consequently, we may conclude that there is high competition between PNP and T-X-100 molecules for the free electrode surface, aggravating flat adsorption of T-X-100. At higher electrode coverage possible reorientation of PNP within the complex layer could be assumed [37] and such process assigned to one of observed fractal peaks.

Organic substances adsorbed on the mercury electrode usually exert an inhibitory influence on the electrochemical processes that take place at the electrode surface due to the steric effects and due to the decrease in the rate constant(s) of the electrode reactions or accompanied chemical reaction(s). One may expect that the electrochemical behavior of the redox system in the presence of the adsorbed layer on the electrode surface is correlated with the microstructure of the layer. Hence, it may be helpful to examine changes in reduction processes of nitrophenols in mixed layers with T-X-100 to better elucidate fine structural transformations of the layers observed by the fractal analysis.

Electroreduction of *o*- and *p*-nitrophenols were studied in the presence of increasing concentrations of T-X-100. Reduction peak current of both nitrophenols is changing depending on the T-X-100 concentration in the solution. Fig. 8 shows dependence of *ac* peak current of the 10^{-4} M ONP (curve 1) and 10^{-4} M PNP (curve 2) on T-X-100 bulk concentration. The electrochemical behavior of ONP in presence of T-X-100 can be separated in three phases. In the first phase, corresponding to lower concentration range of T-X-100 (up to 0.38 mg/dm^3, $\theta < 0.6$, cf. Fig. 4b) the ONP peak current decreases following the increase of θ, due to the effective blocking of the area available for the ONP reduction by the adsorbed T-X-100 molecules. In the second phase ($\theta > 0.6$), the ONP peak current rapidly increases and attains the maximum value of ~ 1.1 μA at $\theta \sim 1$. In the third phase the peak current remains constant in a broad T-X-100 concentration range. In the case of PNP similar behavior of the peak current is observed for a low concentration range of T-X-100. Initial decrease of peak current is followed by abrupt current increase up to a value of ~ 1.1 μA (T-X-100 bulk concentration range of 0.26 - 0.45 mg/dm^3). After reaching the maximum, contrary to the ONP reduction, the peak current of PNP continuously decreases with further increase of T-X-100 bulk concentration. A small increase of currents, observed for both nitrophenols, at T-X-100 bulk concentration of about 6 mg/dm^3, coincides with the adsorption of dimers. These changes of peak current coincide with T-X-100 concentration domains of different *D* values and occurrence of fractal peaks (cf. Fig. 4). Hence, we may conclude that they are indeed correlated to the structural changes of mixed adsorbed layers during their buildup.

The general and simplified scheme of the reduction of nitrophenols at pH 8.3, may be written as follows:

$$Ph\text{-}NO_2 \xleftrightarrow{e^-} Ph - NO_2^{\cdot -} \xrightarrow{e^-, 2H^+, -H_2O} Ph\text{-}NO \xleftrightarrow{2e^-, 2H^+} Ph - NHOH$$

This scheme is really more complicated owing to reactions of protonation and dismutation [38-40]. First step of this scheme shows that nitro group is reversibly reduced in a one-electron reaction to radical anion. Second step is an irreversible reduction to the nitrosophenol, which is further reversibly reduced to the phenylhydroxylamine. In the aqueous medium and on a mercury electrode the reaction of organic compounds such as aromatics practically always occurs via the adsorbed species [40, 41].

At applied experimental conditions reduction of *o*- and *p*-nitrophenols, without T-X-100 is irreversible, as confirmed by *sw* voltammetry (Figs. 9a and b, curves 1).

Fig. 10 shows *ac* voltammograms and corresponding changes of capacitive currents of pure nitrophenols and in the mixture with T-X-100 at few selected concentrations. In the Fig. 10a, curve 1 represents the *ac* voltammogram of 10^{-4} M ONP. In repeated scan on the same mercury drop (curve 1A) a prepeak can be observed. This prepeak represents reversible oxidation of hydroxylamin to nitroso group as confirmed by SW voltammetry (peak *A* in Fig. 9a). The reduction of nitroso group occurs at the potential more positive than the reduction of the corresponding nitro-group [39]. Hence, at used experimental conditions the reduction of ONP is the four-electron reaction up to phenylhydroxylamine.

In the Fig. 10b, curve 1 represents the *ac* voltammogram of 10^{-4} M PNP. In this case the repeated scan at the same mercury drop did not reveal any prepeak, neither at *ac* nor at *SW* voltammetry. This indicates that at chosen experimental conditions PNP is reduced in an irreversible two-electron process.

In the mixed systems, in the low bulk concentration range of T-X-100 the number of electrons partaking in reduction of nitrophenols is unchanged. However, the

electroreduction is more irreversible as indicated by broadening and potential shift of the peaks (curves 2 in Figs 9a and b). For ONP in repeated scan at the same mercury drop the prepeak was observed for all T-X-100 concentrations up to 0.38 mg/dm^3. Hence, it is reasonably to assume that at the low surface coverage with T-X-100 molecules the reduction of nitrophenols still proceeds from the adsorbed state.

In the next narrow concentration range of T-X-100, where the peak currents of both nitrophenols show abrupt increase (cf. Fig. 8), the repeated scan at the same mercury drop did not reveal any prepeak. For both investigated nitrophenols the maximum peak current value is ~ 1.1 μA and the half-peak width is 90 mV. In *ac* voltammetry this corresponds to a reversible one-electron reduction. In *sw* voltammetry the peaks show quasi-reversible behavior (Fig. 9, curves 2) starting at T-X-100 bulk concentrations of 0.55 and 0.44 mg/dm^3 for mixtures with ONP and PNP, respectively, therefore these T-X-100 concentrations were chosen for presentation in Fig. 9. Hence, it may be concluded that in this T-X-100 concentration range the reduction mechanism of nitrophenols has changed from multi-electron irreversible to the one-electron reversible. We suppose that the rate constants of proton and electron transfers in the reduction processes of investigated nitrophenols in T-X-100 layer have decreased rendering first electron reversible reduction to become measurable in the applied experimental window. Similarly, the decrease of the standard rate constants of the $C_6H_5NO_2^{\cdot -}$/ C_6H_5NHOH and C_6H_5NHOH/PhNO processes in the study of nitrobenzene reduction in the presence of increasing concentration of hexamethylphosphotriamide (HMPA) has been observed [42]. At higher surface coverage (T-X-100 bulk concentration up to 10 mg/dm^3) and at given experimental conditions, the reduction of ONP to radical anion remains unchanged indicating enhancement of radical

anion stability in such layers. The enhanced stability of nitrobenzene radical anion was also found in nonionic micelles and was assigned to the surface interactions [43]. In the same concentration range of T-X-100 the first reduction step of PNP undergoes irreversibilization, as manifested in a decrease of peak current as well as peak broadening (Fig. 10b, curve 4).

Observed changes in the reduction mechanism of nitrophenols in the presence of T-X-100 can be related to the microstructure of the adsorbed layer and different orientation of the nitrophenols in the layer. Different orientations of nitroaromatics in the adsorbed layer prefer different pathways of electroreduction. Parallel orientation favors electron acceptance as a first stage of electroreduction while perpendicular orientation in the layer favors protonation of nitro group as a first step [37]. At very low bulk concentration of T-X-100 in the mixture with 10^{-4} M nitrophenol the dominant species adsorbed on the electrode surface is nitrophenol due to its much higher concentration in the bulk. Increase of T-X-100 concentration in this concentration range results in reduction of available space for adsorption and reduction of nitrophenols due to the much higher hydrophobicity of T-X-100. However, the structure of adsorbed layer does not change significantly and reduction mechanism of particular nitrophenol does not change significantly. In this phase flat orientation of adsorbed nitrophenol molecules is probably preferred. In the next narrow T-X-100 concentration range that corresponds to major restructuring of the mixed adsorbed layer, the nitrophenol molecules also very probably change orientation from flat to erected, although not necessarily synchronously with T-X-100 erection. This is indicated by change of reduction mechanism of nitrophenols from multi- to one-electron and also by corresponding appearance of fractal peaks. Similar phenomenon was observed for the

reorientation of *2*-mercaptopyridine *N*-oxide on the mercury electrode in the presence of T-X-100 layer [44]. In the range of high T-X-100 concentration, corresponding to high electrode surface coverage, the fractal dimension of all investigated adsorbed layers is $D \approx 2$, indicating relatively uniform and smooth layers. However, different reduction mechanisms of the two nitrophenols may indicate that ONP partitionates in the layer of nonionic surfactant T-X-100, while PNP does not. The hypothesis that ONP can partitionate in nonionic surfactant phase is supported by previously published evidence of interaction between nitrobenzene radical anion and nonionic micelles [43]. The different affinity for T-X-100 layer between *o*- and *p*-isomers is probably caused by geometrical, steric inhibition of para positioned functional groups on the benzene ring.

4. Conclusions

The study of adsorption processes and structural transformations of simple and mixed adsorbed layers (T-X-100 and T-X-100 with *o*- or *p*-nitrophenol) at the mercury electrode surface has been performed using electrochemical methods and fractal analysis.

Investigation of adsorption process of T-X-100 with classical capacitive current measurements reveals adsorption of monomers and dimers without providing any finer details of the process or involved structural changes of the adsorbed layer. These are provided through diversified approach comprising desorption peak height analysis, fractal analysis, nonthermodynamic calculation of coefficient of lateral interaction, calculation of

relative coverage assuming flat and perpendicular dispositions of molecules, fit of experimental data with two modified Flory-Huggins isotherms and predictions of RSA and equilibrium (generalized RSA) theories.

It appears that fractal analysis is a powerful tool, as fractal dimension is sensitive to subtle structural change(s) of adsorbed layer. Hence, observed specific changes of fractal dimension were assigned to certain structural changes such as saturation, isotropic to nematic transition, erection of initially flatly adsorbed molecules etc.

In conclusion, based on all considerations, the transformation of the adsorbed layer of nonionic surfactant T-X-100 goes through four phases corresponding to different T-X-100 concentration ranges:

- initially, isotropic phase in which the attractive forces between flatly adsorbed molecules are responsible for formation of isotropic patches,
- secondly, the transformation phase characterized by the increase of density in adsorbed layer up to saturation at $\theta_{S(T\text{-}X\text{-}100)} \approx 0.5$, followed by planar nematization at $\theta_{I\text{-}N.} \approx 0.6$, and erection of the molecules,
- thirdly, homogenization phase in which adsorption proceeds with molecules adsorbed in erected position in relatively compact and homogenous layer with $D \approx 2$,
- finally, adsorption of dimers.

At bulk concentration of nitrophenols of 10^{-4} M and potential E = -0.35 V the adsorbed layers of pure nitrophenols do not exhibit fractal properties. However, the mixed layers of T-X-100 with ONP or with PNP have fractal structures that are changing with the increase of T-X-100 bulk concentration. Markedly different fractal dimension of the mixed

systems and observed changes in the reduction mechanisms between the two nitrophenols in the presence of T-X-100, were induced by the corresponding changes in the microstructure of the adsorbed layer. The mixed layer of T-X-100 and ONP is subject to similar changes as that of pure T-X-100, indicating partitioning of ONP in the T-X-100 layer. The mixed layer with PNP exhibits completely different behavior as a consequence of repulsive interactions between PNP and T-X-100 molecules, resulting in expulsion of PNP from the layer at higher coverage, followed by the change of reduction mechanism of PNP that has not been observed for ONP.

Acknowledgement: The authors acknowledge support from the Croatian Ministry of Science, Education and Sport, grants No. 0098122 and No. 0098029.

.

References

[1] D. Risović, B. Gašparović, B. Ćosović, Langmuir 17 (2001) 1088.

[2] L. Pospišil, J. Phys. Chem. 92 (1988) 2501; T. Wandlowski, L. Pospíšil, J. Electroanal. Chem. 270 (1989) 319.

[3] B.B. Mandelbrot, The Fractal Geometry of Nature, Freeman, San Francisco, 1982.

[4] D. Risović, B. Gašparović, B. Ćosović, Colloid. Surface. A, 223 (2003) 145.

[5] D. Risović, B. Gašparović, B. Ćosović J. Phys. Chem.106 (2002) 9810.

[6] D. Hamburger, O.Biham and D. Avnir, Phys. Rev. E, 53 (1996) 3342.

[7] O. Malcai, D.A. Lidar, O. Biham, Phys. Rev. E 56 (1997) 2817.

[8] . D. Avnir, O. Biham, D. Lidar, O. Malcai, Science 279 (1998) 39.; B. Mandelbrot, ibid. p .783. P. Pfeifer, ibid. p.784 , A.A. Tsonis, ibid. p .787.

[9] J. Heyrovsky, P. Zuman, Practical Polarography, Academic Press, New York, 1968.

[10] R. Rodríguez -Amaro, E. Muñoz, J.J. Ruiz, J.L. Avila, L. Camacho, J. Electroanal. Chem. 358 (1992) 127.

[11] E. Sahlin, D. Jagner, Anal. Chim. Acta 333 (1996) 233.

[12] J. Zhang, P.R. Unwin, J. Electroanal. Chem. 494 (2000) 47.

[13] M.S. Romero-Cano, A. Martin-Rodriguez, G. Chauveteau, F.J. de las Nieves, J. Colloid Interface Sci. 198 (1998) 273.

[14] Y. Zeyer, in: A. Bjorseth, G. Angeletti (Eds.), Organic Micropollutants in the Aquatic Environment, Reidel Publishing Company, Doedrecht, 1985; pp. 305-311.

[15] H.L. Keith, W.A. Telliard, Environ. Sci. Technol. 13 (1979) 416.

[16] R.F. Rekker, The hydrophobic fragmental Constant, Elsevier, Amsterdam-Oxford-New York, 1977.

[17] N. Batina, I. Ružić, B. Ćosović, J. Electroanal Chem. 190 (1985) 21.

[18] A. Ray, G.J. Nemethy, Am. Chem. Soc. 93 (1971) 6787.

[19] R.P. Schwarzenbach, R. Stierly, B.R. Folsom, J. Zeyer, Environ. Sci. Technol. 22 (1988) 83.

[20] L. Benedetti, C. Fontanesi, C., Electrochim Acta 39 (1994) 737.

[21] R. De Levie, Chem. Rev. 88 (1988) 599.

[22] C. Buess Herman, in: J. Lipkowski. P.N. Ross. (Eds.), Adsorption of Molecules at Metal Electrodes WCH Publishers, Wellington Cambridge,1992, Ch. 2.

[23] Nikitas, P., J. Electroanal. Chem. 348 (1993) 59.

[24] Nikitas, P.,S. Sotiropoulos, N. Papadopoulos, J. Phys. Chem., 96 (1992) 8453.

[25] H. Jehring, Elektrosorptionanalyse mit Wechelstrom-Polarographie, Akademie, Berlin, 1974, p 135.

[26] B.B. Damaskin, O.A. Petrii, V.V. Batrakov, Adsorption of organic compounds on electrodes; Plenum Press: New York, 1971; Chs. 3 and 4.

[27] R. Guidelli, M. R. Moncelli, J. Electroanal. Chem. 89 (1978) 261.

[28] H.P. Dhar, B.E. Conway and K.M. Joshi, Electrochim.Acta 18 (1973) 789.

[29] A.A. Moussa, H.A.Ghalay, M.M. Abou-Romia and F. El.-Taib Heakal, Electrochim. Acta 20 (1975) 489

[30] R. Parsons, J.Electroanal Chem. 8 (1964) 93.

[31] Munoz, R., Rodriguez-Amaro,J.J. Ruiz, J.L. Avila and L.Camacho, J.Electroanal. Chem. 324 (1992) 359.

[32] M. Carla, G. Aloisi, M. L. Foresti, R. Guidelli, J.Electroanal Chem. 197 (1986) 123.

[33] J. Feder, J. Theor. Biol. 87 (1980) 237.

[34] J. A. Cuesta, D. Frenkel, Phys. Rev. A, 42 (1990) 2126.

[35] G. Tarjus, P. Schaaf, J. Talbot, J. Chem. Phys. 93 (1990) 8352.

[36] D. Risović, B. Gašparović, B. Ćosović, Adsorption of rod-like molecules – fractal aspects, *in preparation.*

[37] B. Kastening, L. Hollec, J. Electroanal. Chem. 27 (1970) 355.

[38] A.M. Heras, J.L. Avila, F. Garcia-Blanco, J. Electroanal. Chem. 170 (1984) 353.

[39] P. Zuman, Z. Fijalek, J. Electroanal. Chem. 296 (1990) 583.

[40] E. Laviron, R. Meunier-Prest, R. Lacasse, J. Electroanal. Chem. 375 (1994) 263.

[41] E. Laviron, J. Electroanal. Chem. 382 (1995) 111.

[42] A. Kalandyk, J. Stroka, J. Electroanal. Chem. 346 (1993) 323.

[43] G.L. McIntire, D.M. Chiappardi, R.L. Casselberry, H.N. Blount, J. Phys. Chem. 86 (1982) 2632.

[44] J.M. Rodriguez Mellado, R. Marin Galvin, Electrochim. Acta 41 (1996) 1479.

Figure captions:

Fig. 1**.** Dependence of the measured capacitive current at –0.35 V *vs*. electrode surface area for pure electrolyte (curve 1) and 0.3 mg/dm^3 T-X-100 (curve 2). Symbols denote experimental points and lines corresponding linear fits. *D* and *R* denote the estimated fractal dimension and the regression coefficient, respectively.

Fig. 2. Differential capacity-potential curves for the bulk Triton-X-100 concentrations: 0.1, 0.4, 0.7 and 5 mg/dm^3 (curves 2-5). Pure electrolyte (curve 1), *o*-nitrophenol (curve ONP) and *p*-nitrophenol (curve PNP). Accumulations time 1 min.

Fig. 3. Desorption peak height vs. bulk concentration of Triton-X-100. Measured data are presented with circles and lines represent approximation with logarithmic function.

Fig. 4. (a) Dependence of the fractal dimensions on bulk Triton-X-100 concentration for the electrode potential E = -0.35 V; (b) The corresponding fractional electrode coverages. Curves 1, 2 and 3 correspond to pure T-X-100, T-X-100 with ONP and T-X-100 with PNP. Symbols denote measurement points while lines represent the fit with B-spline.

Fig. 5. (a) Variation of the coefficient of lateral interaction with T-X-100 bulk concentration, (b) Fractional electrode coverage with horizontally (H) and perpendicularly oriented (P) molecules *vs*. T-X-100 bulk concentration. Symbols denote points calculated from the measured data while lines represent the fit with B-spline.

Fig. 6. Fit of experimental isotherm with two modified Flory-Huggins isotherms corresponding to low and high coverage ranges, denoted F-H 1 and F-H 2, respectively. Symbols denote measurement points while lines represent the fit.

Fig. 7. Dependence of the fractal dimension (curve **D**) and coefficient of lateral interaction (curve **a**) on relative electrode coverage for T-X-100 layer. Experimental points are denoted by symbols and corresponding fits by lines. Arrows denote relative electrode coverage corresponding to the saturation coverage θ_s(RSA) and Isotropic-to-Nematic transition ($\theta_{I\text{-}N}$), as predicted by Monte Carlo simulations for rod-like molecules with aspect ratio k =5.6.

Fig. 8. Dependence of the *o*-nitrophenol (Δ) and *p*-nitrophenol (o) *ac* voltammetric reduction peak currents on the T-X-100 concentration. Symbols denote measurement points while lines represent the fit with B-spline. Accumulation time 1 min.

Fig. 9. *sw* voltammograms of (a) pure 10^{-4} M *o*-nitrophenol (curve 1), second scan at the same mercury drop (curve 1A) and ONP in the presence of 0.55 mg/dm^3 T-X-100 (curve 2) and (b) 10^{-4} M PNP (curve 1) and PNP in the presence of 0.44 mg/dm^3 T-X-100 (curve 2). Curves f – forward current and curves b - backward current. Accumulation time 1 min.

Fig. 10. (a) and (b) show *ac* voltammograms and (a') and (b') corresponding capacitive currents of pure nitrophenols and in the mixture with T-X-100. (a) *ac* voltammograms of 10^{-4} M ONP in the presence of increasing T-X-100 bulk concentration: 0, 0.38 and 5.0 mg/dm^3 T-X-100, curves 1, 2 and 3, respectively. Curves *A* represent second scan at the same mercury drop. Accumulation time 1 min. (b) *ac* voltammograms of 10^{-4} M *p*-nitrophenol in the presence of increasing T-X-100 bulk concentration: 0, 0.26, 0.46 and 3.0 mg/dm^3 T-X-100, curves 1, 2, 3 and 4, respectively. Accumulation time 1 min.

Fig.1.

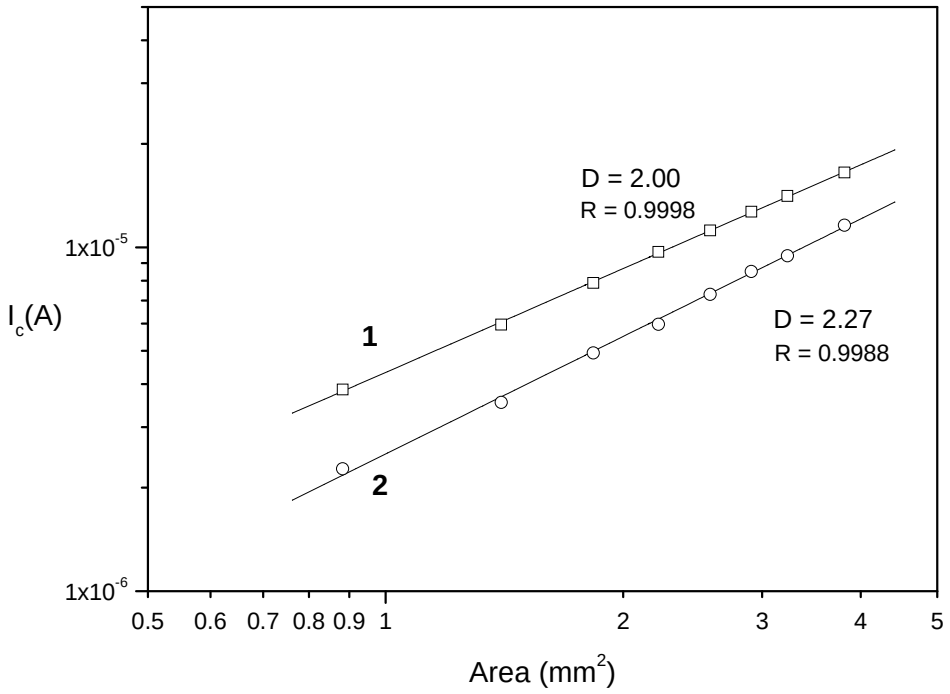
D = 2.00
R = 0.9998
D = 2.27
R = 0.9988
1
2
1x10-5
1x10-6
Ic(A)
0.5
0.6
0.7
0.8
0.9
1
2
3
4
5
Area (mm2)

Fig. 2.

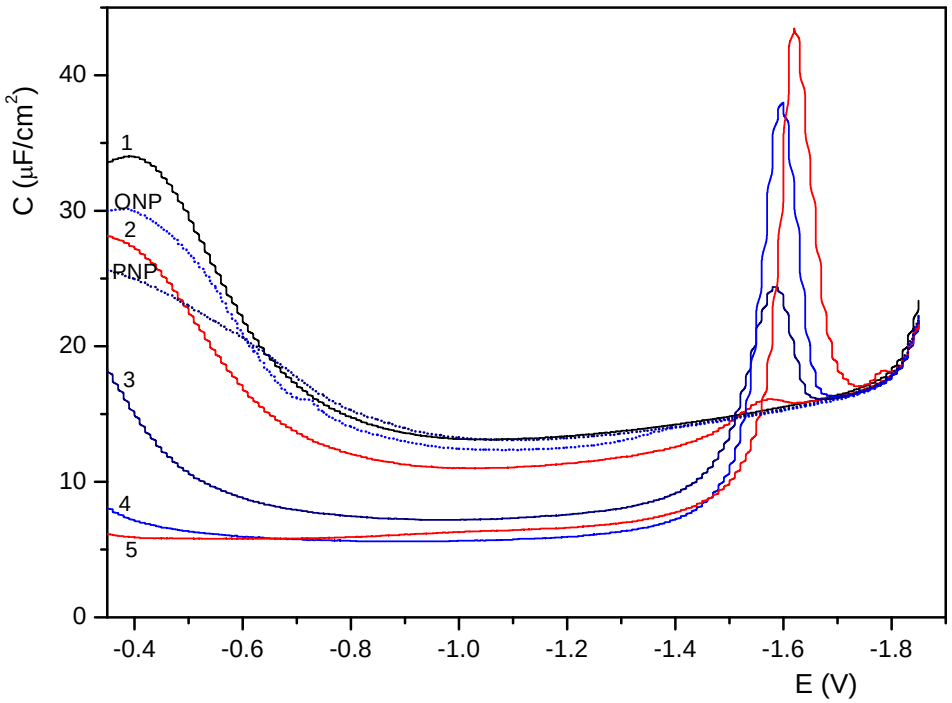

Fig. 3

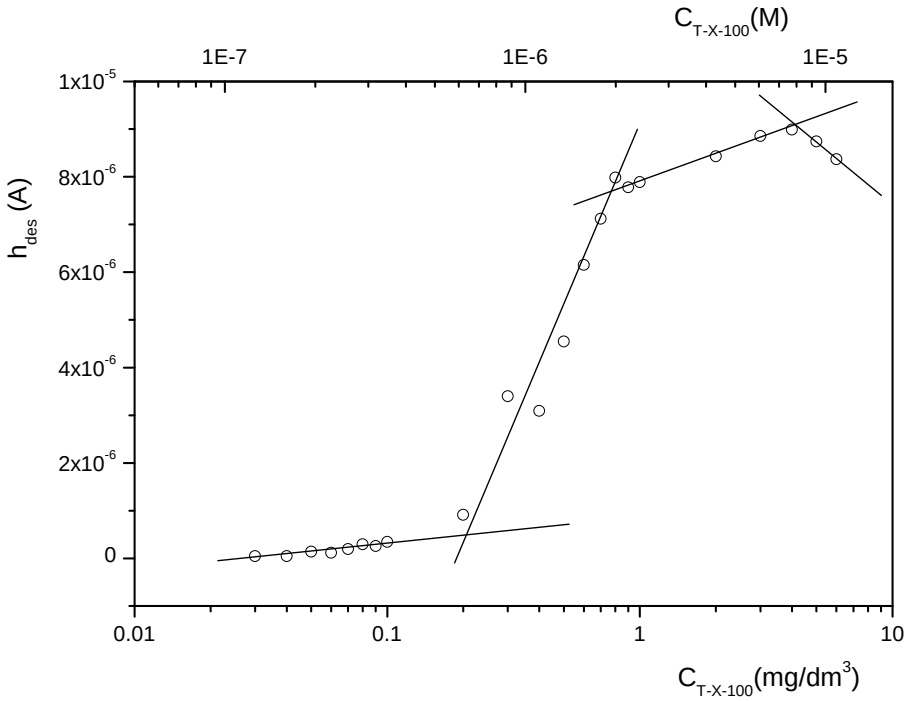
C T-X-100 (M)
1E-7
1E-6
1E-5
1x10-5
8x10-6
6x10-6
4x10-6
2x10-6
0
h des (A)
0.01
0.1
1
10
C T-X-100 (mg/dm3)

Fig. 4

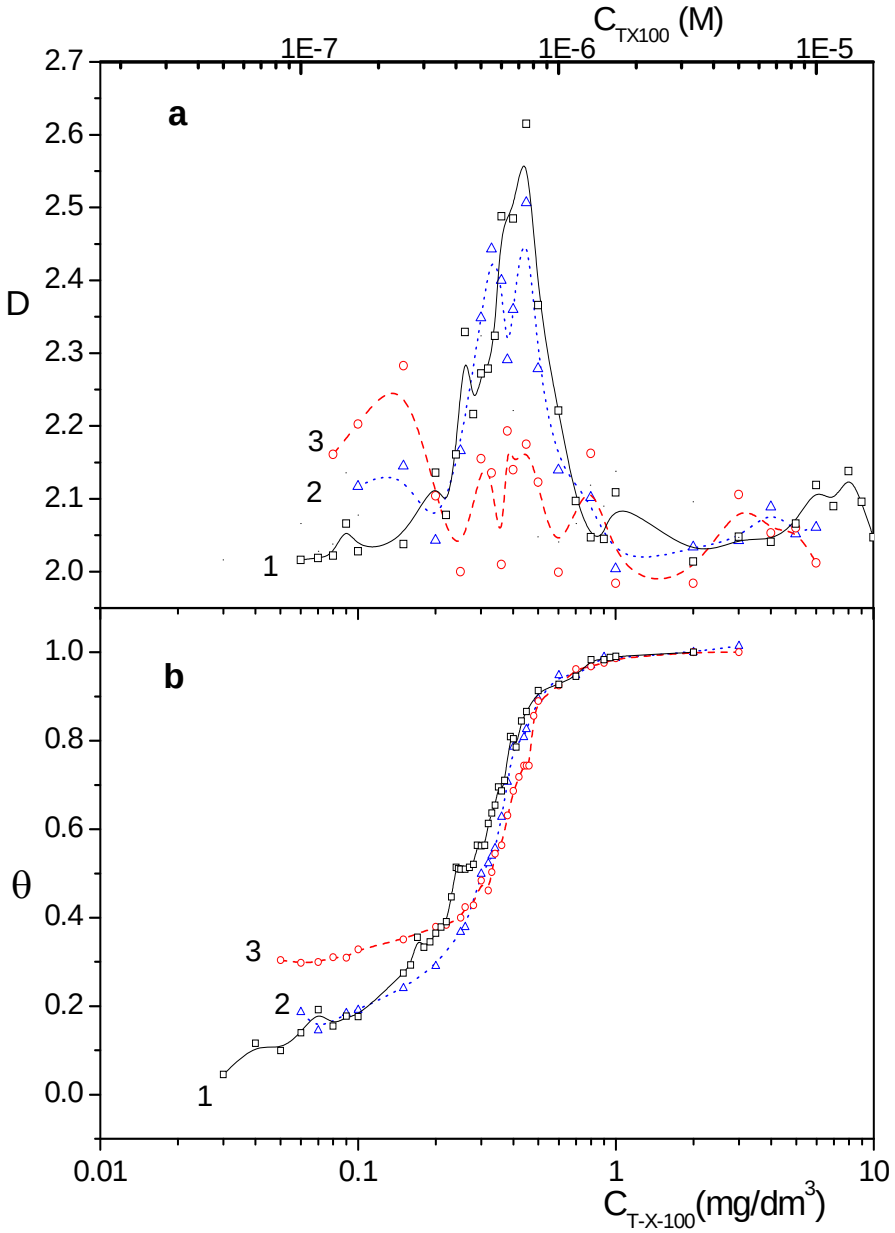
C_TX100 (M)
1E-7
1E-6
1E-5
a
D
2.7
2.6
2.5
2.4
2.3
2.2
2.1
2.0
3
2
1
b
θ
1.0
0.8
0.6
0.4
0.2
0.0
0.01
0.1
1
10
C_T-X-100(mg/dm3)

Fig. 5

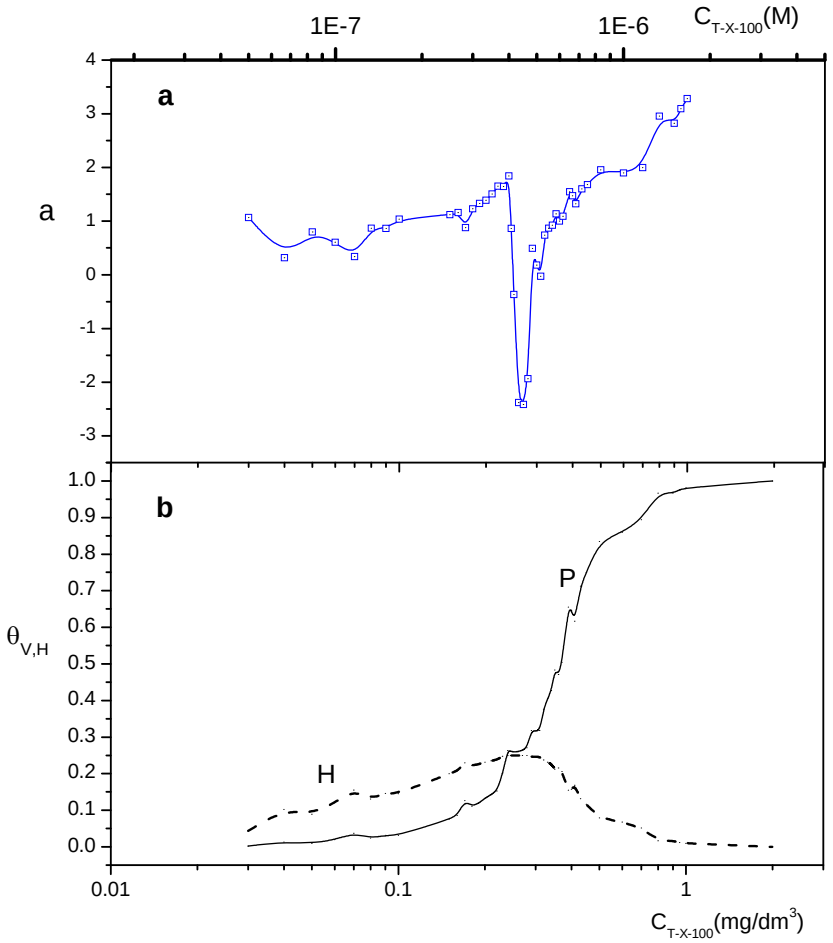

Fig. 6

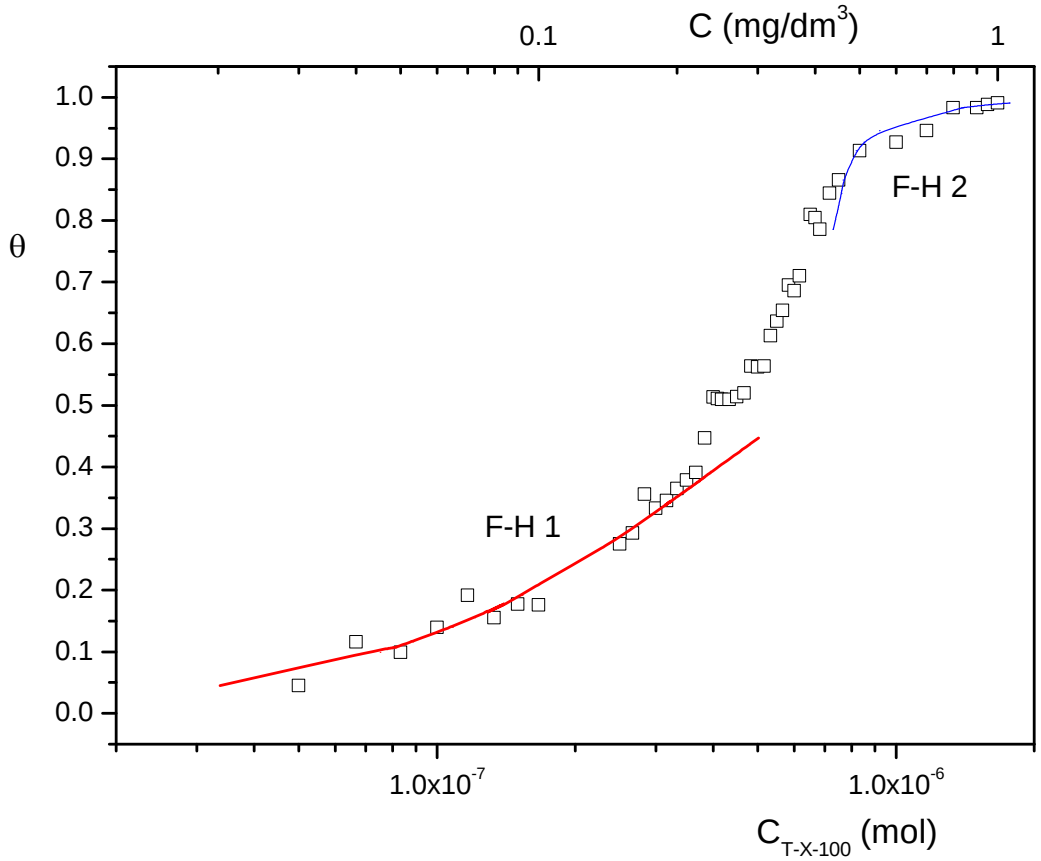
C (mg/dm3)
0.1
1
θ
1.0
0.9
0.8
0.7
0.6
0.5
0.4
0.3
0.2
0.1
0.0
F-H 1
F-H 2
1.0x10-7
1.0x10-6
CT-X-100 (mol)

Fig. 7.

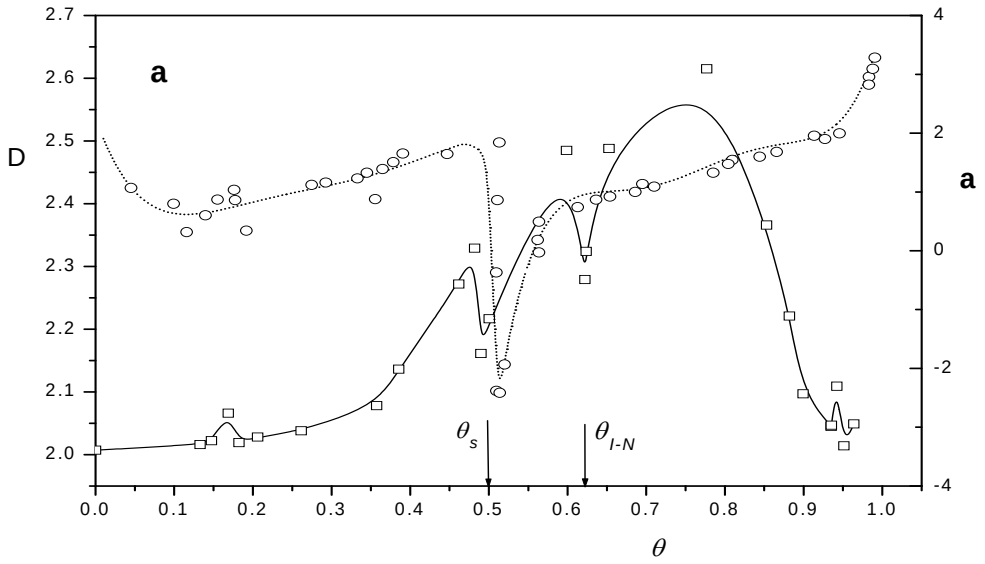
a
D
a
θ
θs
θI-N
2.7
2.6
2.5
2.4
2.3
2.2
2.1
2.0
4
2
0
-2
-4
0.0
0.1
0.2
0.3
0.4
0.5
0.6
0.7
0.8
0.9
1.0

Fig. 8.

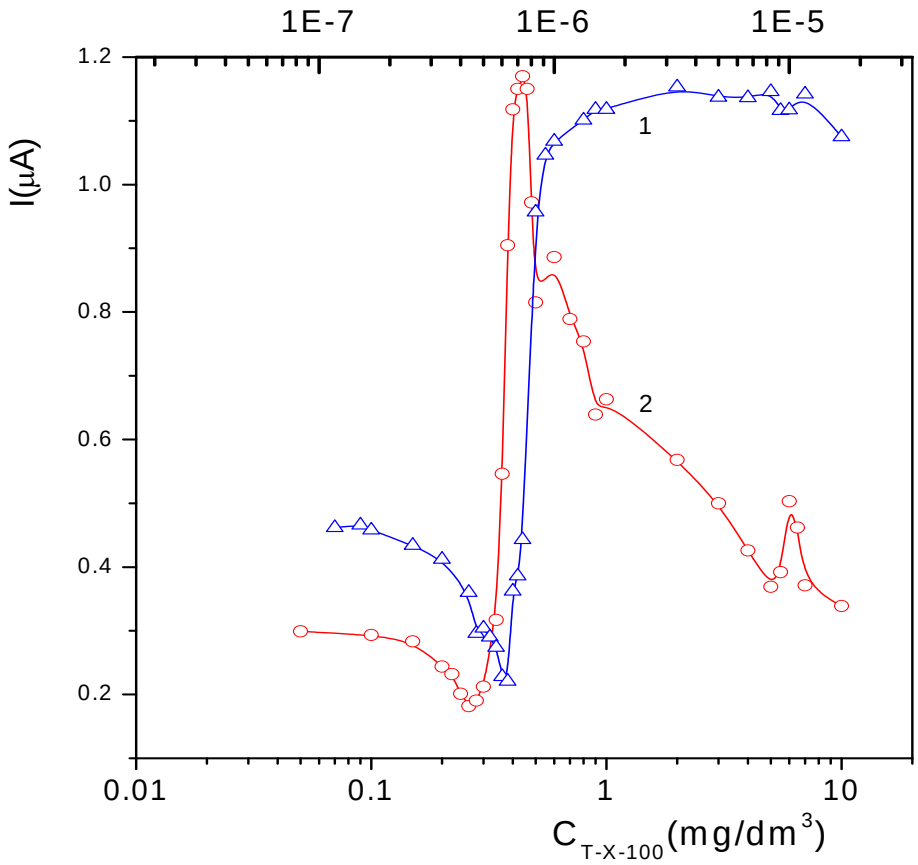

Fig. 9.

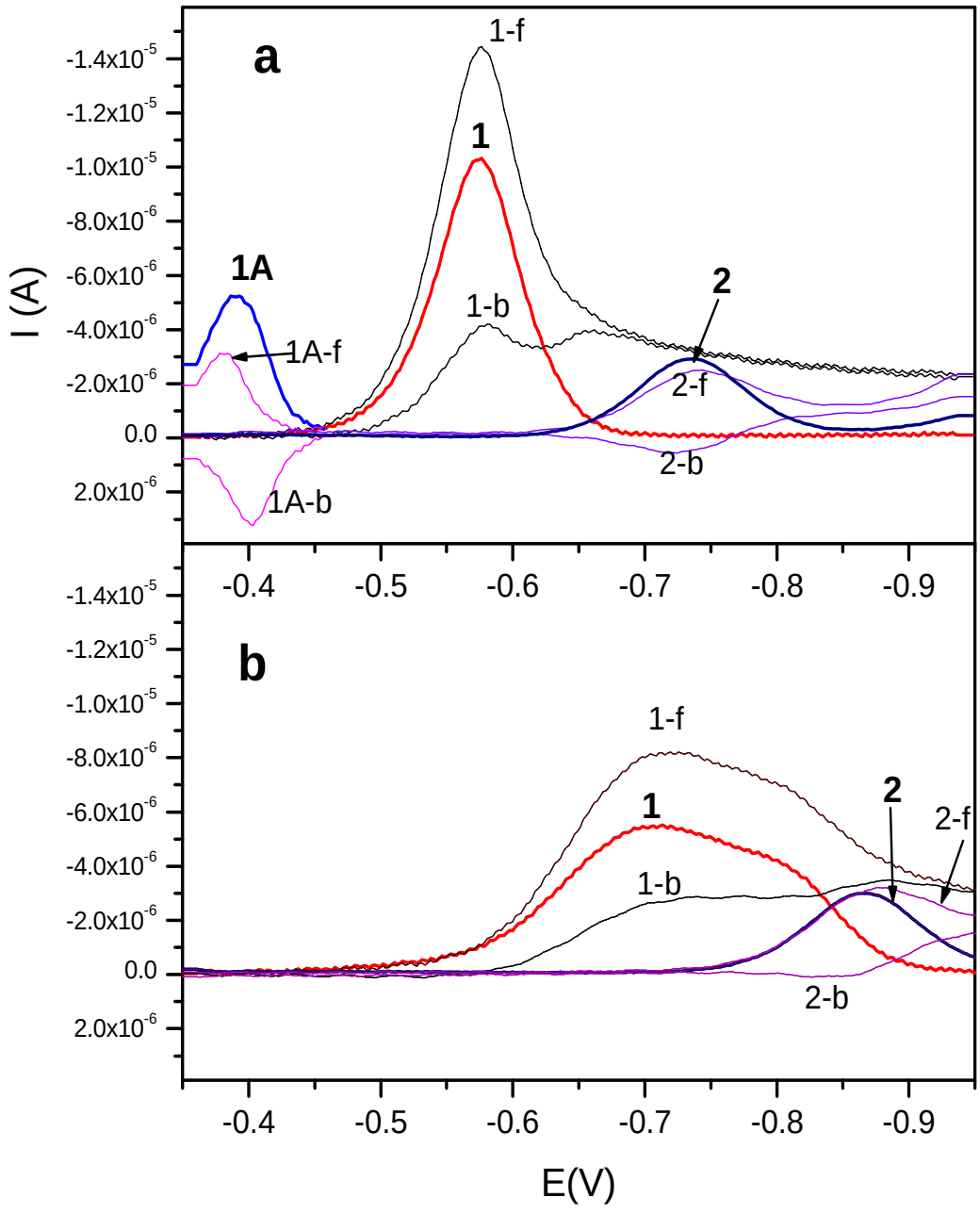
a
b
1-f
1
1A
1-b
2
1A-f
2-f
2-b
1A-b
I (A)
E(V)
-1.4x10-5
-1.2x10-5
-1.0x10-5
-8.0x10-6
-6.0x10-6
-4.0x10-6
-2.0x10-6
0.0
2.0x10-6
-0.4
-0.5
-0.6
-0.7
-0.8
-0.9

Fig. 10.

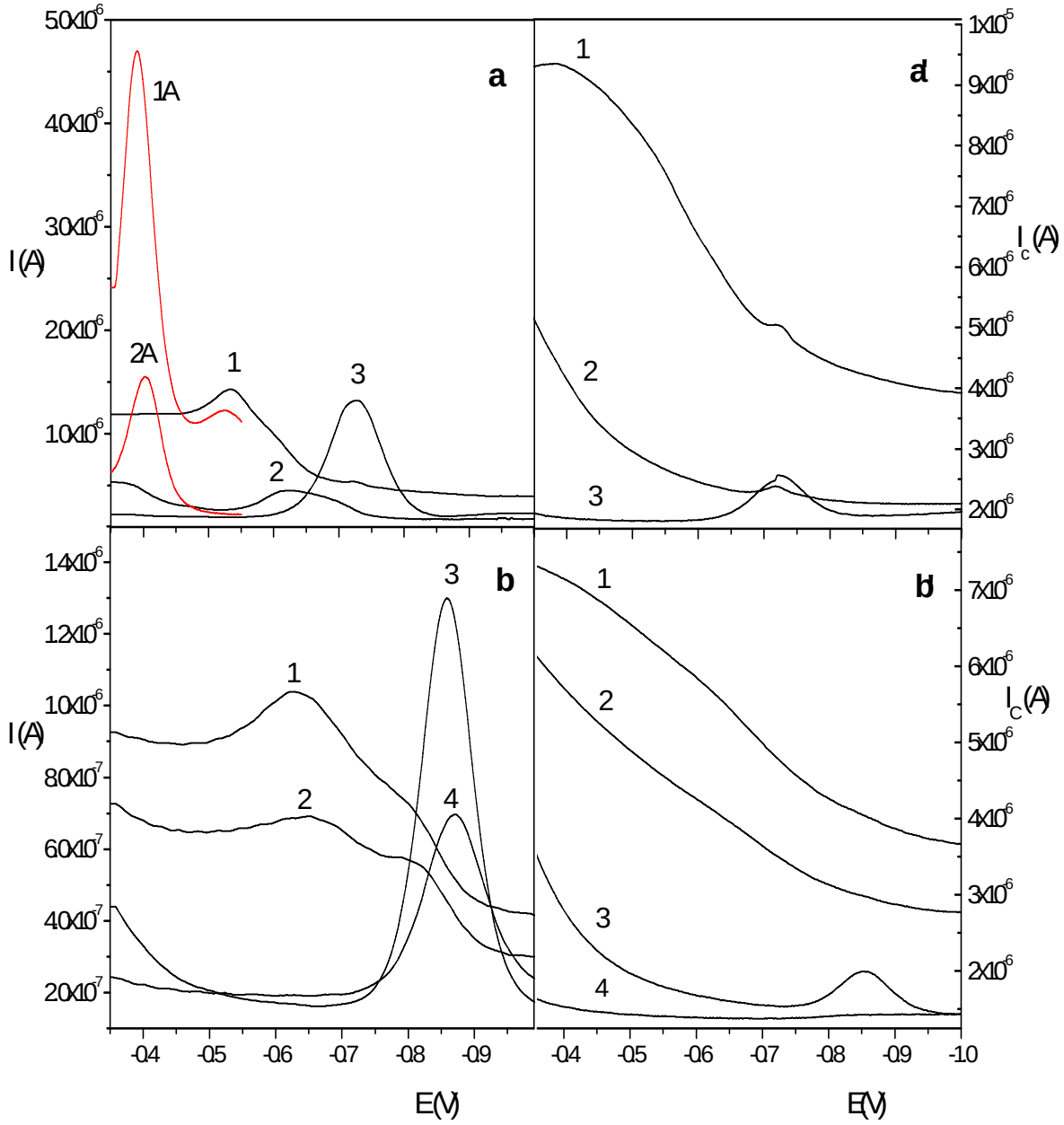
a
a'
b
b'
1A
2A
1
2
3
4
I (A)
I_c (A)
E(V)
50x10^-6
40x10^-6
30x10^-6
20x10^-6
10x10^-6
1x10^-5
9x10^-6
8x10^-6
7x10^-6
6x10^-6
5x10^-6
4x10^-6
3x10^-6
2x10^-6
14x10^-6
12x10^-6
10x10^-6
80x10^-7
60x10^-7
40x10^-7
20x10^-7
7x10^-6
-04
-05
-06
-07
-08
-09
-10